Calculation of TVL and HVL for Shielding Requirements in Radiotherapy Facilities using Monte Carlo Simulation

Dewa Ngurah Yudhi Prasada[1*], Akbar Azzi[2]

[1]Department of Physics, Faculty of Mathematics and Natural Sciences, Universitas Udayana, Badung, Bali, Indonesia 80361
[2]Department of Physics, Faculty of Mathematics and Natural Sciences, Universitas Indonesia, Depok, West Java, Indonesia 16424

Email: *yudhiprasada@unud.ac.id; akbar.azzi@sci.ui.ac.id

Received: 01st July 2025; Revised: 18th July 2025; Accepted: 25th July 2025

Abstract – *Shielding is a critical aspect of radiation therapy facility design to ensure the safety of both workers and the public. This study utilizes the Particle and Heavy Ion Transport System (PHITS) version 3.35 Monte Carlo code to evaluate the tenth-value layer (TVL) of four common materials, like water (1 g/cm³), concrete (2.35 g/cm³), steel (7.8 g/cm³), and lead (11.36 g/cm³), under various photon beam energies of Ir-192 and Co-60 and with various linac energy of 6 MV, 10 MV, and 15 MV, that representing sources typically used in brachytherapy and external beam radiotherapy. The point source, isotropic source, and collimated source were utilized in this research. Results show that TVL values increase with higher beam energy and decrease with denser materials, following the known principles of radiation attenuation. However, an anomaly was observed in lead, where TVL values decreased at energies ≥10 MV, possibly due to pair production effects, which warrants further investigation. None of the results precisely matched the reference values from IAEA SRS-47, likely due to differences in beam spectrum and inherent filtration. These findings suggest that Monte Carlo simulation is a feasible method for estimating shielding requirements, but validation through measurement is recommended.*

Keywords: *Shielding*; *TVL; linear attenuation coefficients; Monte Carlo simulations; radiation protection.*

1. Introduction

Radiation therapy facilities employ high-energy ionizing radiation at high intensities to effectively treat cancer patients. However, the use of such radiation also introduces the potential for significant exposure to surrounding areas if not properly controlled. To ensure safety, the principles of radiation protection, which are time, distance, and shielding, must be rigorously implemented, with shielding playing a particularly critical role in preventing the escape of radiation beyond treatment areas. In Indonesia, the National Nuclear Regulatory Agency (BAPETEN) adopts the recommendations of the International Commission on Radiological Protection (ICRP) Publication 103 [1], which stipulate that the annual dose limit for radiation staff is 20 mSv on average, and for members of the public, 1 mSv. Consequently, the design of radiotherapy facilities must include adequate and effective shielding to ensure compliance with these regulatory limits and to maintain a safe environment for both staff and the public.

The most frequently referenced guideline by medical physicists for designing radiation therapy bunkers is the IAEA Safety Reports Series No. 47 (IAEA SRS-47) [2]. This document provides a comprehensive framework for evaluating radiation doses at specific measurement points outside the treatment bunker, following attenuation by shielding materials of specified thicknesses. The materials most addressed in IAEA SRS-47 are concrete (with a standard density of 2.35 g/cm³), steel, and lead, due to their widespread use and known shielding properties. Additionally, borated polyethylene (BPE) is often used to shield treatment room doors from neutron radiation, especially when high-energy photon beams (>10 MV) are involved. One of the key parameters used in shielding calculations is the tenth-value layer (TVL), which is the thickness of material required to reduce the radiation intensity by a factor of ten. TVL values vary depending on both the shielding material and the energy of the incident photon beam. However, the range of materials covered in IAEA SRS-47 is limited. While heavy concrete, with densities ranging from 4.4 to

5.2 g/cm³, is recommended under certain conditions in NCRP Report No. 151 [3], its TVL values are not explicitly provided in either the IAEA or NCRP publications [2,3].

The determination of TVL for shielding materials can be carried out by systematically varying the material thickness and analyzing the corresponding reduction in radiation intensity, compared to the unshielded (open field) condition. By fitting the attenuation data to an exponential decay model, one can derive the linear attenuation coefficient (μ) of the material [4]. Once μ is known, TVL can be calculated. This method is conceptually straightforward and widely used for low-energy photon sources and low atomic number materials. However, in practical settings, especially involving high-energy photon beams (e.g. >6 MV) or dense materials such as concrete, steel, or lead, this approach becomes technically challenging. The required infrastructure, radiation safety considerations, and detector sensitivity limitations make experimental measurement of TVL values impractical or even infeasible under clinical or laboratory conditions.

To overcome these limitations, Monte Carlo simulations offer a powerful and practical alternative. These simulations use stochastic models to replicate the complex interactions of photons with matter, enabling accurate estimation of radiation transport and attenuation through various materials and geometries. With the ability to simulate a wide range of beam energies, shielding configurations, and material compositions, Monte Carlo codes such as PHITS, Geant4, MCNP, and EGSnrc have become essential tools for calculating TVL values, especially in cases where direct measurement is not viable. Their flexibility and precision make them particularly well-suited for evaluating novel or non-standard shielding materials in radiotherapy facility design [5,6].

Monte Carlo simulations are widely used in radiation therapy, particularly for accurate dose calculation in complex clinical scenarios. These simulations provide a highly detailed modeling of radiation transport by statistically replicating the probabilistic interactions of radiation with matter. This makes Monte Carlo methods especially valuable in cases involving tissue heterogeneity, high dose gradients, or non-standard geometries where conventional algorithms may be insufficient. By accurately modeling photon interactions, such as photoelectric absorption, Compton scattering, and pair production, Monte Carlo simulations contribute significantly to treatment accuracy and patient safety. Beyond dose calculation, one of the most powerful aspects of Monte Carlo simulations is their ability to predict secondary radiation effects, including scattered photons and the production of unintended particles, such as neutrons. Neutron production is particularly relevant in high-energy photon beams (typically above 10 MV) [7], where photonuclear reactions can occur in the linac head or bunker shielding. These secondary neutrons can contribute to increased ambient dose outside the treatment area, potentially exposing radiation workers and the public [8–12]. Monte Carlo tools, such as PHITS, Geant4, and MCNP, are therefore indispensable for evaluating shielding effectiveness, estimating neutron dose contribution, and ensuring compliance with national and international radiation protection standards [13,14].

Furthermore, a growing number of studies have been carried out to evaluate the shielding performance of various materials, emphasizing the importance of accurate modeling of linear attenuation coefficients, half-value layers (HVL), and TVL. For example, research by Alipoor et al. and Malidarre et al. utilized Monte Carlo simulations to investigate the shielding effectiveness of high-performance ultra-heavy cement composites and aluminum-boron-silicate glasses against neutron-gamma mixed radiation fields [15,16]. Many findings are also interesting in shielding properties [17]. In another study, Cui et al. and Hosseini et al. explored the use of rare-earth element/polyethylene terephthalate (REE/PET) composites for broad-spectrum gamma ray protection and B_2O_3-based glass against ionizing radiation [18,19]. These investigations contribute valuable insights into the development of advanced shielding materials, which are critical for ensuring the safety and regulatory compliance of modern radiation therapy facilities at both national and international levels. These findings suggest that the writers evaluate the TVL values in the common materials used in radiation therapy shielding using Monte Carlo simulations.

This study focuses on using the PHITS Monte Carlo [20] code to evaluate the shielding effectiveness of common building materials, such as concrete, steel, lead, and water, against different radiation sources typically used in Indonesian radiotherapy centers. The shielding effectiveness evaluation is limited to responses to the photon source, excluding any other particles. By analyzing the linear attenuation coefficient, HVL, and TVL for various beam types and energies, this work aims to contribute to a more data-driven approach in shielding design, and to assess the feasibility of Monte Carlo simulation as a reliable method for supporting regulatory compliance and clinical safety in Indonesian cancer treatment facilities.

2. Material and Methods

The simulations were carried out using the Particle and Heavy Ion Transport System (PHITS) version 3.35 Monte Carlo code, developed by the Japan Atomic Energy Agency (JAEA) [20]. Three materials commonly used in radiation therapy shielding, which are concrete (density: 2.35 g/cm³), steel (density: 7.80 g/cm³), and lead (density: 11.36 g/cm³), were simulated to determine their HVL and TVL. The concrete was defined using the weight fraction of 1% H, 52.9% O, 1.6% Na, 0.2% Mg, 3.4% Al, 33.7% Si, 1.3% K, 4.4% Ca, and 1.5% Fe. These materials are recommended by both the IAEA SRS-47 and NCRP Report No. 151 for use in radiation therapy shielding. Additionally, water was included in the simulations for comparative purposes. The computer used in these simulations was using Intel Core i5-12500F, with 6 cores and 12 threads. Multithreading options were utilized during the simulations with maximum usage of 8 threads [21]. The total particles used in these simulations ranged from 10^6 – 10^7 particles to reach the minimum statistical errors.

The HVL and TVL values depend on the beam quality, which corresponds to the energy of the incident photon beam. Five different beam qualities were considered in this study: Ir-192, Co-60, 6 MV, 10 MV, and 15 MV. Ir-192 and Co-60 represent commonly used radioactive sources in brachytherapy in Indonesia; Co-60 is also utilized in external beam radiotherapy. The 6 MV, 10 MV, and 15 MV beams represent typical photon energies used in external beam radiation therapy across the country. Three beam types were simulated, including a mono-energy pencil beam with a 0.5 cm radius, an isotropic beam, and a collimated 40×40 cm² broad beam. The isotropic beam used a point source with virtually 0 cm in radius which perfectly simulated the point source. The collimated source was an isotropic point source that was collimated like inside the gantry head of the linear accelerators. These three configurations were analysed to account for differences in scatter radiation, which can influence the resulting HVL and TVL values.

The HVL and TVL values are calculated by determining the linear attenuation coefficient (μ). The μ values can be determined by varying the material thickness and comparing the resulting effective dose (μSv/hr) of the beam at the fixed source-to-detector distance (SDD) with the effective dose without any kind of barrier. We simulated the fixed SDD at 100 cm, with a point detector tally with a defined radius of 0.05 cm. Using the Beer-Lambert relationship, as mentioned in Equation 1, the μ values can be determined.

$$I = I_0 e^{-\mu x} \tag{1}$$

The I and I_0 are the intensity (or in this case, fluence) after passing through the barrier and the initial intensity, respectively. The x value represents the material thickness in cm. As Equation 1 is an exponential relation, the values of μ can be determined using the logarithmic relation between both sides. Equation (1) can be solved by:

$$\frac{I}{I_0} = e^{-\mu x}$$

$$\ln\left(\frac{I}{I_0}\right) = -\mu x$$

$$\ln\left(\frac{I_0}{I}\right) = \mu x \tag{2}$$

As Equation 1 turns into a linear equation in Equation 2, a simple linear regression method can be used to determine the μ values. The μ values related with HVL and TVL since these two values represent the material thickness required to transmit 50% of the initial intensity and 10% of the initial intensity respectively. The relationship between the HVL and TVL with the μ are written in the Equation 3 and 4.

$$\ln\left(\frac{I_0}{\frac{1}{2}I_0}\right) = \mu HVL$$

$$HVL = \frac{\ln 2}{\mu} \tag{3}$$

$$\ln\left(\frac{I_0}{\frac{1}{10}I_0}\right) = \mu TVL$$

$$TVL = \frac{\ln 10}{\mu} \tag{4}$$

3. Result

The results of the simulations are shown in the four sub-sections. The visualizations of the simulation and its dose distribution are also shown below. Before showing the results, Table 1 is the tabulation of TVL values from IAEA SRS 47 document. The HVL value does not need to be shown since it is correlated to each other.

3.1. Visualization of simulation

The visualizations of the simulations are shown in Figure 1. The four figures represent how the simulation performed under the conditions of (a) 20 cm of concrete, (b) 5 cm of lead, (c) 20 cm of water, and (d) 6 cm of steel. Figure 1a and b were used for simulations under the condition of pencil beam and isotropic beam, and Figure 1c and d were used for simulations under the collimated broad beam.

Table 1. The reference value of TVL adopted from IAEA SRS 47 [2].

Materials[a]		TVL Values (cm)				
		Ir-192[b]	Co-60	6 MV	10 MV	15 MV
Concrete	Primary	15.2	21.8	34.3	38.9	43.2
	Secondary		21.8	27.9	30.5	33.0
Steel	Primary	4.3	7.1	9.8	10.5	10.8
	Secondary		6.9	8.0	8.5	8.7
Lead	Primary	1.6	4.1	5.5	5.6	5.7
	Secondary		4.0	4.5	4.6	4.7

[a]The materials stated in IAEA SRS 47 documents have two types of TVL characteristics since the materials are used for external beam radiation therapy shielding. Thus, the primary and secondary beams have different characteristics.
[b]Ir-192 only has one value of TVL since it is commonly used in brachytherapy; therefore, all walls are considered as primary shielding.

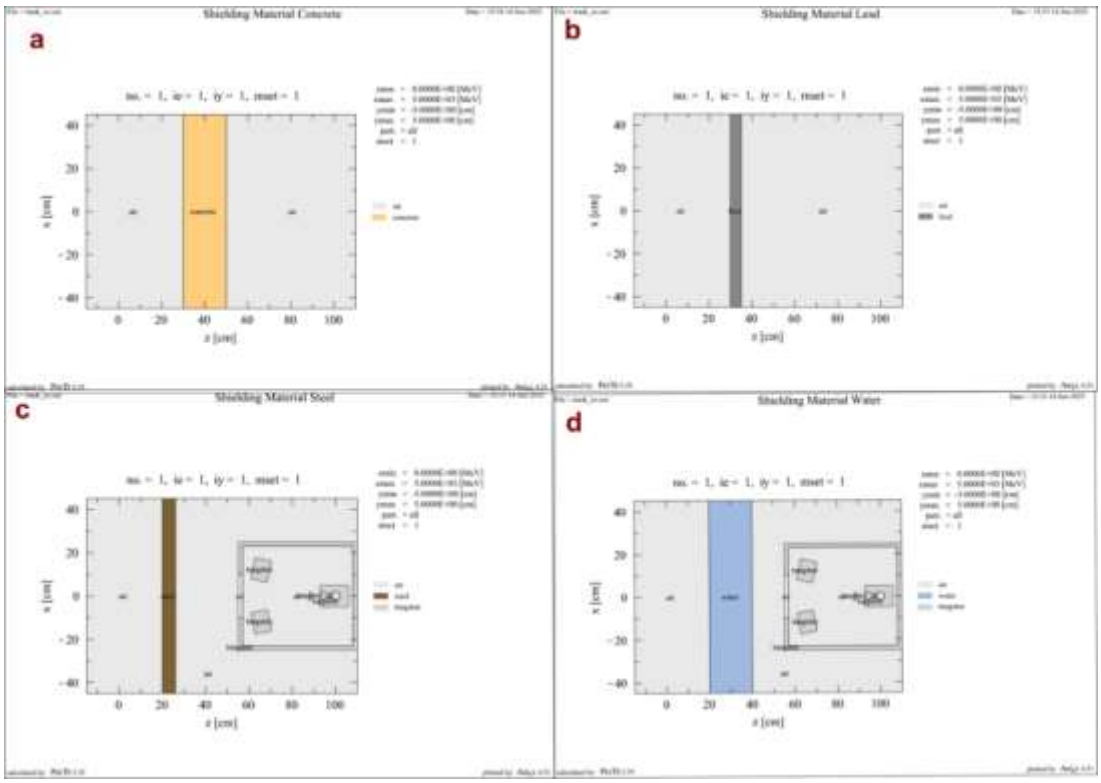

Figure 1. The visualization of the geometry design with various shielding materials of (a) concrete, (b) lead, (c) steel, and (d) water.

3.2. Pencil beam result

The pencil beam results is the representation of how linear attenuation coefficients should be calculated. Beer-lambert's law, as written in Equation 1, is theoretically based on pencil beam attenuation. The

visualization of how the pencil beams move through the materials is expressed in Figure 2. The color scaling in the Figure 2 represents the effective dose in the cross-sectional area of the simulations.

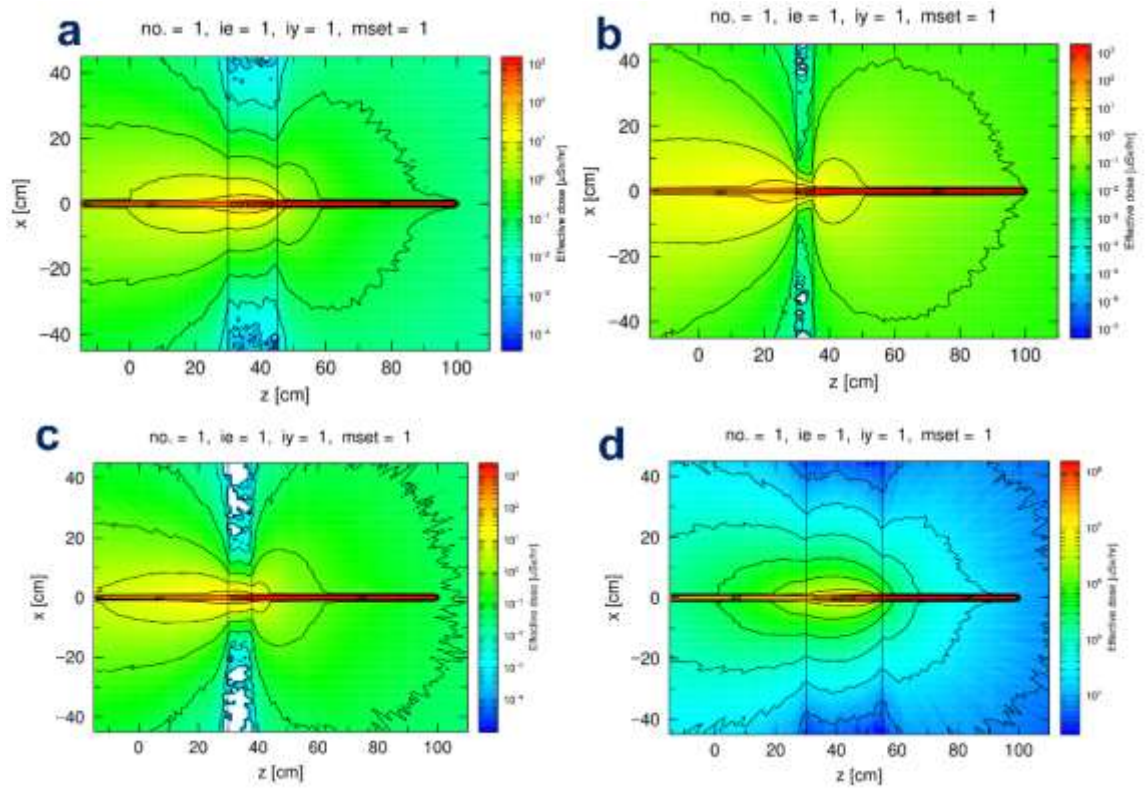

Figure 2. The example visualizations for the pencil simulation move through (a) concrete, (b) lead, (c) steel, and (d) water.

Table 2. The μ, TVL, and HVL values from the simulations with the pencil beam.

Materials	Beam Energy	μ (cm^{-1})	HVL (cm)	TVL (cm)
Water	Ir-192	0.105	6.583	21.867
	Co-60	0.063	11.073	36.783
	6 MV	0.042	16.504	54.823
	10 MV	0.034	20.507	68.124
	15 MV	0.029	24.321	80.792
Concrete	Ir-192	0.219	3.172	10.538
	Co-60	0.133	5.231	17.378
	6 MV	0.087	7.940	26.376
	10 MV	0.072	9.600	31.892
	15 MV	0.063	10.950	36.376
Steel	Ir-192	0.683	1.015	3.371
	Co-60	0.404	1.717	5.705
	6 MV	0.289	2.401	7.976
	10 MV	0.259	2.679	8.901
	15 MV	0.245	2.825	9.383
Lead	Ir-192	1.591	0.436	1.447
	Co-60	0.596	1.164	3.866
	6 MV	0.487	1.422	4.725
	10 MV	0.490	1.415	4.700
	15 MV	0.512	1.353	4.495

Figure 2 shows us how a different beam passes through the different materials with different thickness. All energy and material thickness variations have their own visualizations; however, we only show four figures as in Figure 2 as an example. Figure 2 (a) visualizes the 6 MV beam passing through the 15 cm concrete, (b) visualizes the 10 MV beam passing through the 5 cm lead, (c) visualizes the 15 MV beam passing through 8 cm steel, and (d) visualizes the Co-60 beam passing through the 25 cm of water.

The concrete, lead, steel, and water thickness were varied from 5 – 30 cm, 1 – 5 cm, 2 – 10 cm, and 5 – 30 cm, respectively. Each beam quality was varied with the same variations for materials, and the results are compared with the result with no barrier. Therefore, we have the linear attenuation coefficient (μ) according to Equation 2 using a simple linear regression and Equation 3 and 4 to obtain the HVL and TVL values. The μ, HVL and TVL results for the pencil beam are shown in Table 2.

3.3. Isotropic beam result

The isotropic beam model represents a point source that emits radiation uniformly in all directions. In this model, the radiation dose varies only with the radial distance from the source center. It is commonly used to simulate the behavior of radioactive sources in radiotherapy facilities, particularly in brachytherapy. Although the model assumes isotropic emission, a megavoltage photon beam was also simulated to approximate the contribution of scattered radiation from a linear accelerator (linac). Figure 3 illustrates the interaction of an isotropic beam as it passes through various shielding materials.

Figure 3 (a) visualizes the 6 MV beam passing through the 20 cm concrete, (b) visualizes the 15 MV beam passing through the 4 cm lead, (c) visualizes the Co-60 beam passing through 10 cm steel, and (d) visualizes the Ir-192 beam passing through the 25 cm of water. The same setup with the pencil beam was used in the isotropic beam; therefore, Table 3 shows the μ, HVL, and TVL values of isotropic beam.

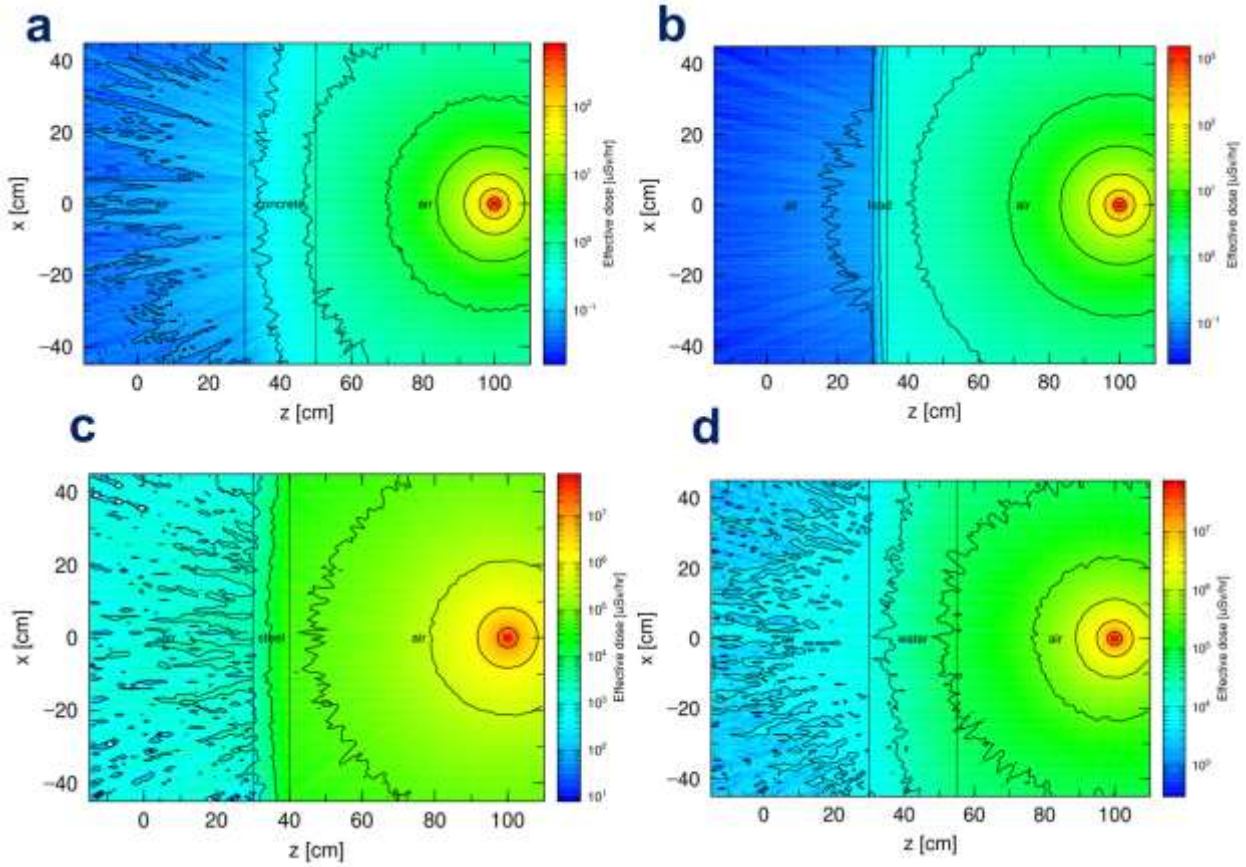

Figure 3. The example visualizations of how the isotropic beam moves through (a) concrete, (b) lead, (c) steel, and (d) water.

Table 3. The μ, TVL, and HVL values from the simulations with the isotropic beam.

Materials	Beam Energy	μ (cm^{-1})	HVL (cm)	TVL (cm)
Water	Ir-192	0.052	13.407	44.537
	Co-60	0.034	20.387	67.723
	6 MV	0.025	27.506	91.372
	10 MV	0.021	32.696	108.613
	15 MV	0.019	36.674	121.830
Concrete	Ir-192	0.145	4.784	15.891
	Co-60	0.087	7.940	26.376
	6 MV	0.061	11.419	37.934
	10 MV	0.052	13.407	44.537
	15 MV	0.047	14.779	49.096
Steel	Ir-192	0.508	1.363	4.529
	Co-60	0.282	2.456	8.159
	6 MV	0.209	3.324	11.044
	10 MV	0.193	3.601	11.961
	15 MV	0.191	3.629	12.055
Lead	Ir-192	1.456	0.476	1.582
	Co-60	0.516	1.344	4.466
	6 MV	0.404	1.716	5.701
	10 MV	0.412	1.681	5.583
	15 MV	0.445	1.558	5.174

3.4. Broad beam result

The collimated broad beam simulations are designed to represent how shielding materials respond to radiation emitted from teletherapy machines or linear accelerators (linacs). In this setup, the broad beam originates from an initially isotropic source but is shaped by the collimation system of the linac head, which includes components such as the flattening filter and jaws. These components provide inherent beam filtration, resulting in a modified energy spectrum compared to the uncollimated beam. In this study, all clinically relevant photon beam energies were simulated, except for Ir-192, as this radionuclide is not used in teletherapy. Figure 4 illustrates the interaction of the collimated beam as it passes through various shielding materials.

Figure 4 (a) visualizes the 6 MV beam passing through the 30 cm concrete, (b) visualizes the 10 MV beam passing through the 5 cm lead, (c) visualizes the 15 MV beam passing through 10 cm steel, and (d) visualizes the Co-60 beam passing through the 30 cm of water. The same setup with the pencil beam was used in the isotropic beam, therefore, Table 4 shows the μ, HVL, and TVL values of the collimated broad beam.

4. Discussion

The simulation results exhibit trends consistent with the expected behavior of photon beams as they pass through various materials. The linear attenuation coefficient (μ) is a material-dependent value influenced by both the density of the shielding material and the energy of the incident photon beam. In terms of increasing density, the materials analyzed follow the order: water, concrete, steel, and lead. For the photon beam energies, the order from lowest to highest is Ir-192, Co-60, 6 MV, 10 MV, and 15 MV. We simulated the water materials as a comparison with another materials. As expected, the water has the lowest linear attenuation coefficient in all conditions, or in other words, has the highest HVL and TVL values.

In general, the HVL (half-value layer) and TVL (tenth-value layer) values increase with higher photon energy. This is expected, as higher-energy photons are more penetrating and less likely to interact with matter, resulting in a lower linear attenuation coefficient. Since HVL and TVL are inversely proportional to μ, a decrease in μ leads to higher HVL and TVL values. Conversely, for a given beam energy, HVL and TVL tend to decrease as material density increases. This is because denser materials present a higher

probability of photon interaction (via photoelectric effect, Compton scattering, or pair production), thus increasing μ and consequently reducing the HVL and TVL.

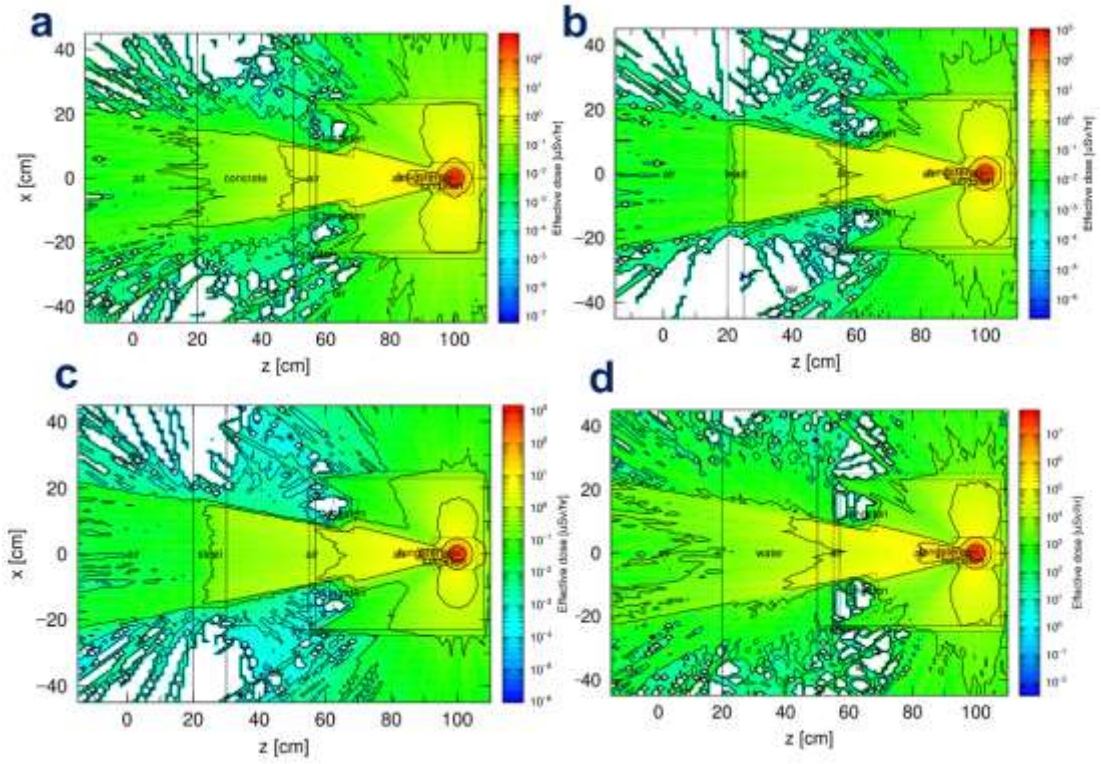

Figure 4. The example visualizations of how the collimated broad beam moves through (a) concrete, (b) lead, (c) steel, and (d) water.

Table 4. The μ, TVL, and HVL values from the simulations with the collimated broad beam.

Materials	Beam Energy	μ (cm^{-1})	HVL (cm)	TVL (cm)
Water	Ir-192	-	-	-
	Co-60	0.028	24.844	82.530
	6 MV	0.024	28.881	95.941
	10 MV	0.020	34.314	113.989
	15 MV	0.018	38.085	126.516
Concrete	Ir-192	-	-	-
	Co-60	0.084	8.222	27.314
	6 MV	0.058	12.055	40.045
	10 MV	0.049	14.088	46.801
	15 MV	0.044	15.753	52.331
Steel	Ir-192	-	-	-
	Co-60	0.250	2.770	9.203
	6 MV	0.191	3.637	12.081
	10 MV	0.179	3.879	12.885
	15 MV	0.177	3.927	13.046
Lead	Ir-192	-	-	-
	Co-60	0.461	1.503	4.993
	6 MV	0.365	1.899	6.308
	10 MV	0.383	1.812	6.018
	15 MV	0.412	1.683	5.590

However, an anomaly was observed in the case of lead at 10 MV and 15 MV. In this case, the simulated TVL values were lower than those observed for 6 MV, which contradicts the expected trend. One possible explanation is the increased probability of pair production interactions, triplet production, or production any elementary particles that have short half-life in lead at higher photon energies, which could enhance the attenuation and result in a higher linear attenuation coefficient. Nevertheless, this finding contradicts the reference values reported in IAEA SRS-47 [2], suggesting the need for further investigation and validation through additional simulations or experimental data.

Another important aspect to discuss is how different beam characteristics influence the calculated HVL and TVL values. While the pencil beam is typically used to determine the linear attenuation coefficient due to its idealized nature, this study also simulated two additional beam types, isotropic and collimated broad beams, to more accurately represent clinical conditions such as brachytherapy sources, scattered radiation, and linac outputs. Several studies have simulated mono-energy narrow photon beam with different beam quality such as Co-60 in various material and MC user codes [22,23]. For the water density, the HVL and TVL in this study were double compared to the narrow beam. The simulation results reveal that, even at the same beam energy, the HVL and TVL values vary across different beam types. The pencil beam represents an ideal scenario where beam intensity does not diminish with distance from the source, i.e., it is independent of geometric divergence. In contrast, both isotropic and collimated beams exhibit intensity attenuation with increasing distance from the source, in accordance with the inverse square law, making them more realistic representations of clinical radiation fields. In general, the HVL and TVL values tend to be higher for the collimated broad beam, especially for low density material. This result agreed with Zaurari et al that for Ir-192 the significant difference of photon transmission between pencil and broad beam was found on concrete rather than lead material [24]. While the pencil beam preserves the original energy spectrum of the source, the isotropic and collimated beams are subject to inherent filtration by components such as shielding materials and collimators, which remove lower-energy photons and increase the mean energy of the beam. This increase in mean energy leads to a reduction in the linear attenuation coefficient (μ), thereby resulting in higher HVL and TVL values.

None of the simulation results in this study exactly match the values reported in IAEA SRS-47. The pencil beam simulations tend to underestimate the HVL and TVL compared to IAEA SRS-47 [2], while the isotropic and collimated broad beam simulations may overestimate these values. According to the IAEA SRS-47, the reported TVL values are derived from data involving large attenuation conditions, as referenced from Nelson et al. [25]. Under large attenuation, the beam's energy spectrum is significantly altered due to inherent filtration, meaning that the spectrum beyond the shielding no longer represents the original beam spectrum.

This spectral hardening effect, particularly in polychromatic beams such as those produced by linear accelerators, leads to an increase in mean photon energy after attenuation, as lower-energy photons are more readily absorbed. Consequently, the linear attenuation coefficient decreases, and the resulting HVL and TVL increase. Another reference of interest is NCRP Report No. 151 [3], which distinguishes between two TVL values for the primary beam: TVL1, representing the attenuation required for the first 90% dose reduction, and TVLe, used for subsequent reductions. This distinction also arises from the evolving energy spectrum of the beam as it penetrates deeper into the shielding material. However, there are some critics with the usage of the Nelson et al. [25], findings that the spectrum used in that research is outdated and might underestimate the TVL result. The result given by McDermott (2023) [26] shows that the concrete TVL_1 for 6, 10, and 15 MV are 41.7, 44.7, and 49.2 cm, respectively. This result approaches our results for the collimated broad beam; however, our results are still a bit higher.

It is important to note that the results presented here are preliminary findings based on simulations using the PHITS Monte Carlo code. For design and regulatory purposes, we recommend using the TVL values provided in IAEA SRS-47 and/or NCRP Report 151, which are based on established empirical and theoretical data. Due to the complexity of replicating clinical beam geometries, such as pencil or isotropic beams with polychromatic x-rays, in experimental setups, direct measurement is practically not feasible. Therefore, future research should involve comparative simulations using other established Monte Carlo codes such as Geant4, MCNP, or EGSnrc, to validate and cross-check the PHITS results. Additionally, the photon beam spectra in future studies should be corrected to match the conditions described by Nelson et al., to more accurately simulate large attenuation scenarios as used in IAEA SRS-47.

5. Conclusion

Monte Carlo simulations using the PHITS code were performed to determine the linear attenuation coefficient, half-value layer (HVL), and tenth-value layer (TVL) of various shielding materials commonly used in radiotherapy facilities. The photon energies simulated ranged from Ir-192 and Co-60 (commonly used in brachytherapy) to 6 MV, 10 MV, and 15 MV beams typically used in external beam radiotherapy. While the results exhibited general consistency with expected physical trends, such as increased HVL and TVL with higher photon energies and lower material densities, discrepancies were found when compared to reference values from IAEA SRS-47. In some cases, TVL values were underestimated (notably with pencil beam simulations), while others showed overestimation (as with isotropic and collimated beam setups), likely due to differences in spectral hardening and inherent filtration effects. Despite these variations, the study confirms that Monte Carlo simulations remain a powerful and feasible approach for evaluating radiation shielding, particularly when experimental measurement is impractical. However, to ensure greater accuracy and consistency, further studies using alternative Monte Carlo transport codes such as Geant4, MCNP, or EGSnrc are recommended, along with adjustments to beam spectra that replicate large attenuation conditions as described in the literature.

Acknowledgement

The authors would like to thank Mr. Tatsuhiko Sato, Mr. Tatsuhiko Ogawa, Mr. Takuya Furuta, and others PHITS development team of the Japan Atomic Energy Agency (JAEA) for guiding and supporting the authors with the PHITS tutorials. The authors would also like to thank the JAEA for supporting the authors with travel funding for attending the PHITS Workshop 2025 in JAEA Mirae Base, Tokai-mura, Ibaraki, Japan. The authors have gained a great deal of new insight and experience with PHITS coding from the event. The authors would also like to thank Iqbal Auliarachman from the Center for Medical Physics and Biophysics, Universitas Indonesia, who served as the discussion partner and provided computational assistance.

References

[1] International Commission on Radiological Protection, ICRP Publication 103: The 2007 Recommendations of the International Commission on Radiological Protection, 2007.
[2] International Atomic Energy Agency, Safety Reports Series No. 47: Radiation Protection in the Design of Radiotherapy Facilities, (2006).
[3] National Council on Radiation Protection and Measurements, NCRP Report No. 151: Structural Shielding Design and Evaluation for Megavoltage X- and Gamma-Ray Radiotherapy Facilities : Recommendations of the National Council on Radiation Protection and Measurements, National Council on Radiation Protection & Measurements, 2006.
[4] A. Akkaş, Determination of the tenth and half value layer thickness of concretes with different densities, in: Acta Phys Pol A, Polish Academy of Sciences, 2016: pp. 770–772. https://doi.org/10.12693/APhysPolA.129.770.
[5] R. Khanna, Y. Reinwald, R.P. Hugtenburg, A. Bertolet, A. Serjouei, Review of the geometrical developments in GEANT4-DNA: From a biological perspective, Reviews in Physics 13 (2025). https://doi.org/10.1016/j.revip.2025.100110.
[6] W. Tseng, K. Furutani, C. Beltran, B. Lu, An automation of Monte Carlo workflow for dosimetry study of an Elekta LINAC delivery system in radiotherapy, Tech Innov Patient Support Radiat Oncol 31 (2024). https://doi.org/10.1016/j.tipsro.2024.100257.
[7] S. Yani, M.F. Rhani, R.C.X. Soh, F. Haryanto, I. Arif, Monte carlo simulation of varian clinac iX 10 MV photon beam for small field dosimetry, International Journal of Radiation Research 15 (2017) 275–282. https://doi.org/10.18869/acadpub.ijrr.15.3.275.
[8] P.V. Cerón Ramírez, J.A.I. Díaz Góngora, L.C. Paredes Gutiérrez, T. Rivera Montalvo, H.R. Vega Carrillo, Neutron H*(10) estimation and measurements around 18 MV linac, Applied Radiation and Isotopes 117 (2016) 2–7. https://doi.org/10.1016/j.apradiso.2016.05.006.
[9] E. Hosseinzadeh, N. Banaee, H.A. Nedaie, Monte Carlo calculation of photo-neutron dose produced by circular cones at 18 MV photon beams, Reports of Practical Oncology and Radiotherapy 23 (2018) 39–46. https://doi.org/10.1016/j.rpor.2017.12.001.

[10] H. Nedaie, H. Darestani, N. Banaee, N. Shagholi, K. Mohammadi, A. Shahvar, E. Bayat, Neutron dose measurements of Varian and Elekta linacs by TLD600 and TLD700 dosimeters and comparison with MCNP calculations, J Med Phys 39 (2014) 10–17. https://doi.org/10.4103/0971-6203.125476.
[11] H.R. Vega-Carrillo, S.A. Martínez-Ovalle, A.M. Lallena, G.A. Mercado, J.L. Benites-Rengifo, Neutron and photon spectra in LINACs, Applied Radiation and Isotopes 71 (2012) 75–80. https://doi.org/10.1016/j.apradiso.2012.03.034.
[12] D.N.Y. Prasada, N. Ciamaudi, M. Fadli, R. Tursinah, S.A. Pawiro, Evaluation of the linac neutron dose profile for various depths and field sizes: A Monte Carlo study, Biomed Phys Eng Express 7 (2021). https://doi.org/10.1088/2057-1976/ac2dd5.
[13] J.A. de la Torre, I. Ruiz-Garcia, D. Guirado, A.J. Palma, M.A. Carvajal, A.M. Lallena, M. Anguiano, A Monte Carlo analysis of the feasibility of a 3D structure build up with silicon photodiodes for in vivo dosimetry in radiotherapy, Radiation Physics and Chemistry (2025) 113012. https://doi.org/10.1016/j.radphyschem.2025.113012.
[14] G. Mckinney, Review of Monte Carlo All-Particle Transport Codes and Overview of Recent MCNPX Features, 2006. https://www.researchgate.net/publication/228894113.
[15] M. Alipoor, M. Eshghi, R. Sever, Monte Carlo Simulation of Gamma and Neutron Shielding with High-performance Ultra-heavy Cement Composite, J Med Phys 49 (2024) 661–672. https://doi.org/10.4103/jmp.jmp_91_24.
[16] R. Boodaghi Malidarre, I. Akkurt, T. Kavas, Monte Carlo simulation on shielding properties of neutron-gamma from 252Cf source for Alumino-Boro-Silicate glasses, Radiation Physics and Chemistry 186 (2021). https://doi.org/10.1016/j.radphyschem.2021.109540.
[17] U. Kara, S.A.M. Issa, G. Susoy, M. Rashad, E. Kavaz, N.Y. Yorgun, H.O. Tekin, Synergistic effect of serpentine mineral on Li2B4O7 glasses: optical, structural and nuclear radiation shielding properties, Appl Phys A Mater Sci Process 126 (2020). https://doi.org/10.1007/s00339-020-3397-8.
[18] H. Hosseini Sarteshnizi, H. Zaki Dizaji, Monte Carlo investigation of the shielding performance of B2O3-based glasses against ionizing radiation, Sci Rep 15 (2025). https://doi.org/10.1038/s41598-025-01916-0.
[19] T. Cui, R. Chen, S. Bi, R. Wang, Z. Ma, Q. Jia, Monte Carlo simulation and study of REE/PET composites with wide γ-ray protection, Nuclear Engineering and Technology 55 (2023) 2919–2926. https://doi.org/10.1016/j.net.2023.04.030.
[20] T. Sato, Y. Iwamoto, S. Hashimoto, T. Ogawa, T. Furuta, S.I. Abe, T. Kai, Y. Matsuya, N. Matsuda, Y. Hirata, T. Sekikawa, L. Yao, P.E. Tsai, H.N. Ratliff, H. Iwase, Y. Sakaki, K. Sugihara, N. Shigyo, L. Sihver, K. Niita, Recent improvements of the particle and heavy ion transport code system–PHITS version 3.33, J Nucl Sci Technol 61 (2024) 127–135. https://doi.org/10.1080/00223131.2023.2275736.
[21] M.C. Han, Y.S. Yeom, H.S. Lee, B. Shin, C.H. Kim, T. Furuta, Multi-threading performance of Geant4, MCNP6, and PHITS Monte Carlo codes for tetrahedral-mesh geometry, Phys Med Biol 63 (2018). https://doi.org/10.1088/1361-6560/aabd20.
[22] O. Gundogdu, U.A. Tarim, O. Gurler, Monte Carlo Calculations for Photon Attenuation Studies on Different Solid Phantom Materials, Acta Phys Pol A 132 (2017) 1032–1035. https://doi.org/10.12693/APhysPolA.132.1032.
[23] H. Hosseini Sarteshnizi, H. Zaki Dizaji, Monte Carlo investigation of the shielding performance of B2O3-based glasses against ionizing radiation, Sci Rep 15 (2025) 17595. https://doi.org/10.1038/s41598-025-01916-0.
[24] K. Zourari, V. Peppa, F. Ballester, F. Siebert, P. Papagiannis, Brachytherapy structural shielding calculations using Monte Carlo generated, monoenergetic data, Med Phys 41 (2014). https://doi.org/10.1118/1.4868456.
[25] W.R. Nelson, P.D. LaRIVIERE, Primary and Leakage Radiation Calculations at 6, 10 and 25 MeV, Health Phys 47 (1984) 811–818.
[26] P.N. McDermott, Linac primary barrier transmission for concrete: Monte Carlo calculations, J Appl Clin Med Phys 24 (2023). https://doi.org/10.1002/acm2.13847.